Global and Planetary Change 133 (2015) 346–358

Contents lists available at ScienceDirect

Global and Planetary Change

journal homepage: www.elsevier.com/locate/gloplacha

The Badenian–Sarmatian Extinction Event in the Carpathian foredeep basin of Romania: Paleogeographic changes in the Paratethys domain

Dan V. Palcu [a,*], Maria Tulbure [b], Milos Bartol [c], Tanja J. Kouwenhoven [b], Wout Krijgsman [a]

[a] Paleomagnetic Laboratory "Fort Hoofddijk," Utrecht University, Budapestlaan 17, 3584 CD, Utrecht, The Netherlands
[b] Department of Earth Sciences, Utrecht University, Budapestlaan 4, 3584 CD, Utrecht, The Netherlands
[c] Department of Earth Sciences, University of Uppsala, Villav. 16, 75236 Uppsala, Sweden

ARTICLE INFO

Article history:
Received 30 April 2015
Received in revised form 13 August 2015
Accepted 24 August 2015
Available online 5 September 2015

Keywords:
Paratethys
Biostratigraphy
Magnetostratigraphy
Extinction
Paleogeography
Gateways

ABSTRACT

The Badenian–Sarmatian boundary interval is marked by a major extinction event of marine species in the Central Paratethys. The exact age of the boundary is debated because many successions in marginal basins show erosional features and fauna reworking at the boundary level. Here, we selected the Tisa section in the Carpathian foredeep basin of Romania, which is continuous across this Badenian–Sarmatian Extinction Event (BSEE). Quantitative biostratigraphic records of planktic and benthic foraminifera and calcareous nannofossils allow to accurately locate the Badenian–Sarmatian boundary and indicate a major paleoenvironmental change from open marine to brackish water conditions. Magnetostratigraphic results reveal a polarity pattern that uniquely correlates to the time interval between 12.8 and 12.2 Ma. Interpolation of constant sedimentation rates determines the age of the BSEE in the Carpathian foredeep at 12.65 ± 0.01 Ma, in good agreement with several earlier estimates. We conclude that the extinction event took place in less than 10 kyr, and that it was most likely synchronous across the Central Paratethys. It corresponds to a major paleogeographic change in basin connectivity with the Eastern Paratethys, during which the nature of the Barlad gateway switched from a passive to a full connection.

1. Introduction

Paratethys represents the large epicontinental sea that extended from Central Europe to inner Asia since the Oligocene (Laskarev, 1924). This realm was characterized by progressive fragmentation and isolation from the global ocean, as a direct consequence of the continental collision that shaped the Alpine–Himalayan orogenic belt (Rögl, 1998). The region was segregated into smaller basins that were clustered in three paleogeographic units: Western, Central and Eastern Paratethys. The short-lived Western Paratethys comprised the Alpine Foreland Basins of France, Switzerland, South Germany and Upper Austria (Senes, 1961) and disappeared by the end of the Early Miocene. Central Paratethys was located in what is today Central Europe (Fig. 1) from Middle Miocene to Pliocene (Cicha and Seneš, 1968; Papp et al., 1968) while Eastern Paratethys was located in the Black Sea – Caspian Sea and – Aral Sea area (Fig. 1a) from the Oligocene onwards (Popov et al., 2006).

Recurrent fragmentation of the Paratethys and repeated isolation of individual sub-basins led to the development of endemic biota. The resulting fossil assemblages led to the introduction of regional chronostratigraphic subdivisions, because direct biostratigraphic correlation to the standard Geological Time Scale (GTS) is generally not possible (Piller et al., 2007). Chronological frameworks for Paratethys sub-regions should preferentially be combined with independent magnetostratigraphic and radio-isotopic age determinations. Such integrated stratigraphic studies that allow direct correlations to the GTS have so far only been developed for restricted intervals (Vasiliev et al., 2004; Vasiliev et al., 2005; Hohenegger et al., 2009a; Krijgsman et al., 2010; Vasiliev et al., 2010; Paulissen et al., 2011; Vasiliev et al., 2011; Reichenbacher et al., 2013; ter Borgh et al., 2013; Van Baak et al., 2013; Hohenegger et al., 2009a; Krijgsman et al., 2010; Paulissen et al., 2011).

Here, we focus on the extinction event that can be observed at the boundary of the Badenian and Sarmatian ages of the Central Paratethys. The Badenian–Sarmatian Extinction Event (BSEE) (Harzhauser and Piller, 2007) is a catastrophic event that marks a turning point in the history of Paratethys (Harzhauser and Piller, 2004). The BSEE is the largest faunal turnover event in the Paratethys realm with a 94% extinction of Badenian species including a full loss of coral, radiolarian and echinoid life forms from Central Paratethys (Harzhauser and Piller, 2007). It is recognized throughout the entire Central Paratethys and is correlated with the Konkian–Volhynian boundary of Eastern Paratethys (Fig. 2); (Popov et al., 2013).

Existing age estimates for the BSEE do not fully agree with each other (Table 1, Fig. 2). They range from an age of 12.7 Ma based on correlations to global sea level low stands (Harzhauser and Piller, 2004) to an astronomically dated age of 13.32 Ma (Lirer et al., 2009). Most of these

* Corresponding author.
E-mail address: d.v.palcu@uu.n (D.V. Palcu).

http://dx.doi.org/10.1016/j.gloplacha.2015.08.014
0921-8181/

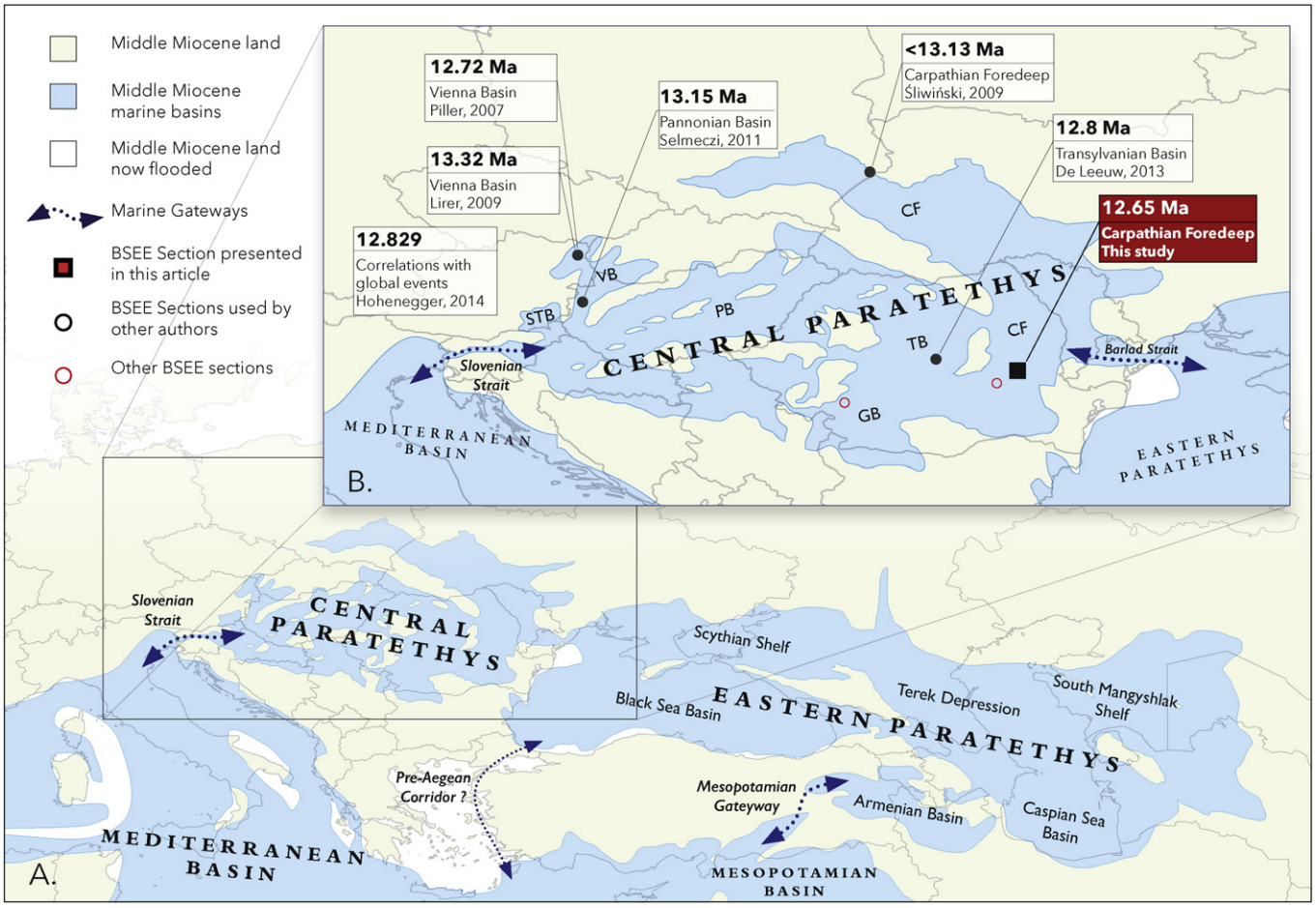

Fig. 1. (A) Simplified paleogeographic reconstruction of the Mediterranean–Paratethys region during the late Badenian (modified after Popov et al., 2006), overlain on the present day map contours, marked in gray. (B) Simplified paleogeographic reconstruction of Central Paratethys with dated BSEE sections. Abbreviations for the relevant Central Paratethys sub-basins: CF — Carpathian Foredeep, PB — Pannonian Basin, TB — Transylvanian Basin, VB — Vienna Basin, STB — Styrian Basin, and GB — Getic Basin.

age models rely on geological data from the shallow, marginal sub-basins from the westernmost part of Central Paratethys (Fig. 1b) where the BSEE level is marked by a widespread discordance in the sedimentary record.

In this paper, we present a chronological framework for the Badenian to Sarmatian succession from the deeper facies sedimentary record of the Romanian Carpathian Foredeep basin, based on the integration of biostratigraphy and magnetostratigraphy. The results will provide another step forward in the discrimination of global climate (eustatic sea level lowering) versus regional tectonics (orogenic uplift or basin reconfiguration) causing the BSEE.

2. Paleogeographic and geologic background

We have focused our research on the area in front of the SE Carpathian Bend where a very deep basin (Focsani Depression) developed in Miocene to recent times (Tarapoanca et al., 2003). This basin had a pivotal location from biogeographic point of view. It was situated in the easternmost part of Central Paratethys for most of the middle Miocene (Fig. 1) and became part of Eastern Paratethys, during the Sarmatian. This paleogeographic change is related to collisional tectonics in the Carpathian region, in conjunction with the subduction of the Eastern European Platform underneath the Tisza–Dacia plate (Matenco et al., 2010).

We selected one continuous sedimentary succession with a good biostratigraphic record and good quality paleomagnetic signal. This section is on the Tisa Valley (45° 17.565′ N, 26° 29.567′ E), a tributary of Bălăneasa River in the Buzau River Catchment. Lithologically, siliciclastic rocks, evaporites and tuffites characterize the Tisa Valley sediments. The succession begins with middle Badenian evaporites (halite) and salt breccia and is followed by upper Badenian clays rich in organic matter (Radiolarian shales) and marls with sand intercalations (Spirialis marls). The lower Sarmatian record is almost entirely composed of marls, occasionally containing well-cemented sandy laminae and some sandy levels. Five thin, tuffitic levels have also been recognized. Sampling has focused on the upper part of the Badenian (above the levels identified as Radiolarian shales) and the Sarmatian in the small Tisa stream bed, where the succession was almost continuously exposed.

3. Integrated bio-magnetostratigraphy

The section was logged (with on average sampling interval of 2 m) and the resulting lithological column shows a sequence of sediments characterized by coarse silts, fining upwards to marls with several intercalations of sands and volcanic ashes (Fig. 3). In the middle part of the section (66–71 m), numerous sapropelic intercalations and a thin horizon with volcanic ash stand out. Further above (150 m), levels with *Ervilia* sp. molluscs indicate a Sarmatian age and place the BSEE lower than 150 m. Consequently the biostratigraphic sampling has focused on the lower part of the section (0–160 m) where the extinction event was located while the magnetostratigraphic sampling range covered the entire section (0–222 m) to provide a longer paleomagnetic polarity pattern that would allow a better correlation to the GPTS.

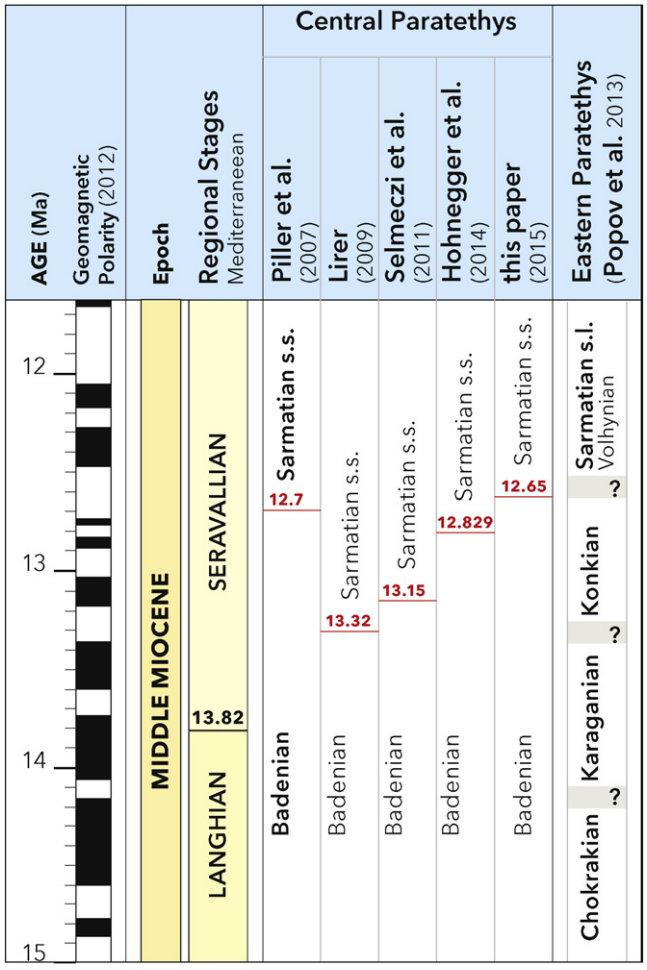

Fig. 2. The age estimates developed for the BSEE in the Central Paratethys and corresponding stratigraphy of the Eastern Paratethys.

3.1. Foraminifera

A total number of 63 samples from the homogeneous marls of the Tisa Valley section have been analyzed for planktic and benthic foraminifera to document the biostratigraphy and paleoenvironmental changes across the Badenian–Sarmatian boundary interval. The samples were dried at room temperature, disintegrated in water and washed over a 125 μm sieve. The washed residues were split using an Otto Microsplitter to obtain aliquots containing 200–300 benthic foraminifera. Planktic foraminifera are preferentially used for biostratigraphy, but in regional studies, benthic foraminifera have proven to be useful when planktic foraminifera are absent (Popescu, 1995; Crihan, 1999). In addition, variations in the benthic foraminifera assemblage represent paleoenvironmental conditions of the Tisa section. A stratigraphic distribution chart expresses the evolution of the foraminiferal assemblage (Fig. 3).

3.1.1. Planktic foraminifera

The preservation of the foraminifera is generally good with the exception of some short intervals where microfauna is scarce or samples are sterile. At the levels where microfauna is absent, the detrital component consists of pyrite, quartz, gypsum, and silts with glauconite, biotite and muscovite, revealing short anoxic episodes. Planktonic foraminifera are abundant in the Badenian, where in some levels they reach up to almost 100% of the total number of foraminifera (e.g. TS24, TS25). This part also contains some reworked planktic foraminifera from the Cretaceous (*Globotruncana* sp. — TS1 and TS8) and the lower Serravallian (Badenian) such as *Candorbulina* sp., *Velapertina* (syn. *Praeorbulina* sp.; TS1). The Badenian planktonic assemblage consists mainly of species of the *Globigerina bulloides* group, in which we include both *Globigerina praebulloides* and *G. bulloides* taxa. The presence of *Praeorbulina* sp. (syn. *Velapertina*; TS1) together with a high number of *Globigerina concinna* (Reuss, 1850) and *Globigerina tarchanensis* (Subbotina, and Chutzieva, 1950) indicates that this part of the section correlates to the upper Badenian (Dumitrica et al. 1975; Popescu, 1999; Popescu and Crihan, 2011). At approximately 68.4 m (between TS25 and TS26), the planktic foraminifera completely disappear and only benthic fauna remains (red line in Fig. 3). This event takes place within a 120 cm interval, indicating a sudden dramatic environmental change in the basin.

3.1.2. Benthic foraminifera

The preservation of benthic foraminifera is generally good except for a short interval (69.8–79.8 m) characterized by crushed benthonic foraminifera or small shells. In the upper part of the section (from 80 m upwards) the preservation improves again. The benthic foraminifera assemblage of the lowermost 59.4 m is dominated by two species: *Martinottiella communis* and *Valvulineria complanata* (Fig. 3). A more diverse fauna, including *Quinqueloculina regularis*, *Sigmoilinita tenuis*, *Sphaeroidina variabilis*, *Bolivina dilatata* and *Bulimina* (syn. *Baggatella*) *subulata*, characterizes the interval between 61.2 and 67.8 m. Above the 69 m level all the previously mentioned species disappear and are

Table 1
Age estimates developed for the BSEE, with their dating methods and limitations. Note that most of these estimates are based on records with hiatuses at or straddling the BSEE.

The BSEE age models				
Nr.	Age	Author	Method	Limitations
1.	12.829 Ma	Hohenegger et al. (2014)	Correlations between third sea-level cycle (TB 2.5 after Haq et al. 1988) and magnetostratigraphy to the top of polarity Chron C5Ar.2n (Ogg 2012)	Hiatus in the record at the BSEE level
2.	12.80 Ma	De Leeuw et al. (2013)	Bio-magneto-stratigraphy in the Transylvanian Basin	Hiatus in the data at the BSEE level — low resolution
3.	13.15 Ma	Selmeczi et al. (2012)	Bio-magneto-stratigraphy on drill cores	Hiatus in the record at the BSEE level
4.	12.735–12.474 Ma	Paulissen et al. (2011)	Correlations of the BSEE with the C5Ar.1r	Hiatuses and difficulties in correlations at the BSEE levels
5.	13.32 Ma	Lirer et al. (2009)	Astronomical dating by correlation between an orbital tuned Middle and early Late Miocene record of the Central Paratethys and an astronomically calibrated Mediterranean deep marine composite record	Not excluded that the well-data was obscured by a hiatus at that crucial level
6.	<13.13 Ma	Śliwiński (2012)	Radiometric dating of ash levels older than the BSEE	Insufficient constraints to provide an age
7.	12.73 Ma	Hohenegger et al. (2009b)	Correlation with the recalculated Third-order sequence TB2.6 of Haq et al. (1988)	Hiatus in the record at the BSEE level
8.	12.72 Ma	Piller et al. (2007)	Correlations with sea level low stands such as the glacio-eustatic isotope event MSi-3 (Abreu and Haddad, 1998)	Hiatus in the record at the BSEE level
9.	13.00 Ma	Westerhold et al. (2005)	Correlations with the benthic foraminiferal δ18O to the Mi4 event — one of the short periods of glaciation in the Miocene (Mi-events) described by Miller et al. (1991)	Hiatus in the record at the BSEE level

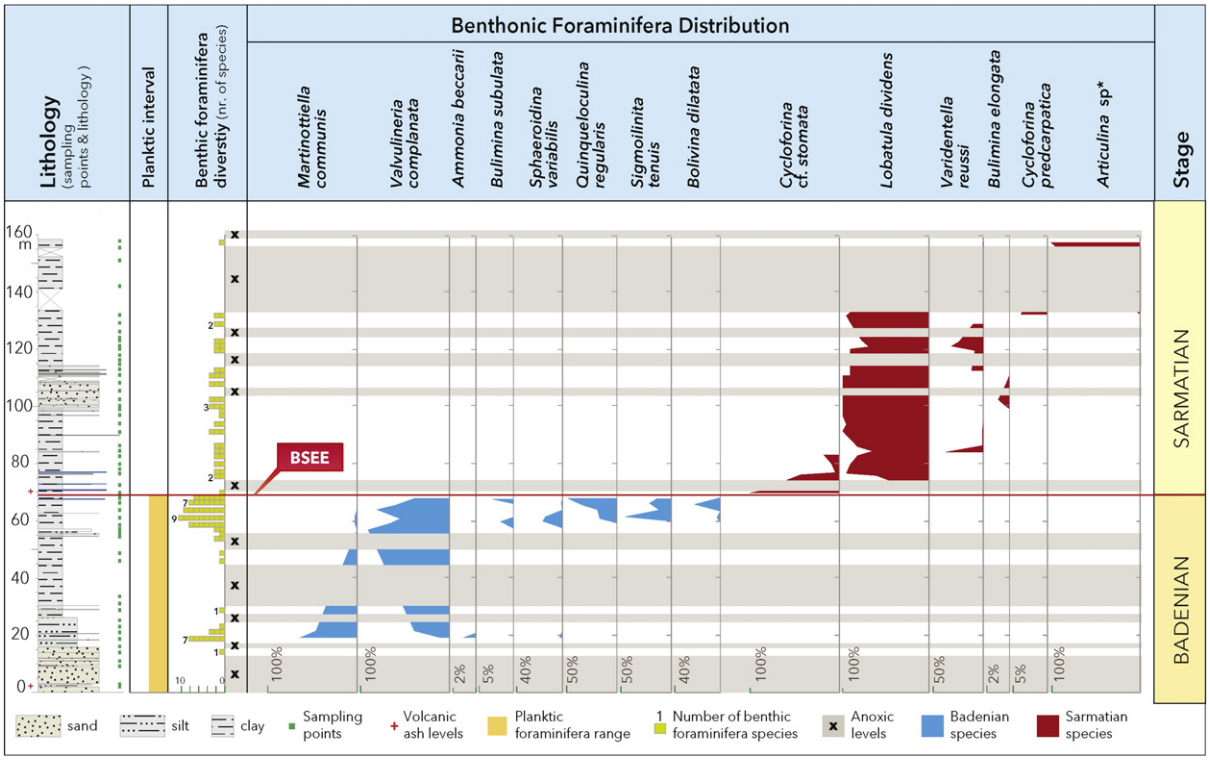

Fig. 3. Quantitative distribution of relevant benthic foraminifera taxa against the lithostratigraphy of the Tisa section. Please note differences in scaling. The yellow column indicates the stratigraphic interval with planktic forams. Gray bands indicate barren, anoxic levels. BSEE line indicates the stratigraphic level where the Badenian–Sarmatian Extinction Event has been identified based on the foraminifera data.

replaced by *Cycloforina stomata* (Łuczkowska, 1974; Crihan, 2002) and *Lobatula* (syn. *Anomalinoides*) *dividens*. Upwards in the section other species progressively appear and increase the diversity: *Varidentella* (syn. *Miliolina*) *reussi* (82 m), *Bulimina elongata* (99 m), *Cycloforina predcarpatica* (128 m) and *Articulina* sp. (160 m). The Badenian species *Q. regularis* as well as the Sarmatian markers *C. stomata* and *Varidentella reussi* are indicative of relatively deep basinal settings (Łuczkowska, 1974). Several barren samples have been found at the levels 2.9–11 m, 16 m, 25.3 m, 31.1–33.8 m, 55.6 m, 105.3 m, 114.8–117.9 m, 124–126 m, and 151–167 m. These barren levels are characterized by the presence of fish bones, otholits, pyrite and biotite and some pyritized micro-gastropod fossils seem to suggest lowered levels of oxygen.

3.1.3. The Badenian–Sarmatian boundary interval

The benthonic foraminiferal assemblages of the lower part of the section are well known from Paratethys literature and are attributed to the upper Badenian (Popescu, 1979). The assemblages of the upper part of the section clearly correspond to the *Lobatula dividens* zone, which is the lowermost biostratigraphic zone of the Sarmatian (Popescu, 1999). Consequently, this allows us to place the Badenian–Sarmatian boundary between samples TS25 and TS26, corresponding to the interval 67.8–69.0 m in the Tisa section. This interval marks the sudden disappearance of Badenian taxa, including planktic species and the gradual onset of the Sarmatian fauna, which is dominated by miliolids. Whereas the Badenian assemblages contain taxa confined to normal marine salinity, the Sarmatian assemblages are characteristic by brackish conditions, indicating that water chemistry changed at the extinction level of the Badenian taxa (Popescu, 1979).

3.2. Calcareous nannoplankton

For nannofossil assemblage analyses we prepared standard microscope slides from marl samples and quantitatively analyzed them under a light microscope by counting all specimens until the total of more than 300. Species with documented last occurrences before the Middle Miocene were counted separately. This method underestimates the proportion of reworked specimens — as reworked specimens of species with long stratigraphical ranges extending into the studied time interval cannot be distinguished from autochthonous specimens. Still this method provides a good estimate of the extent of reworking in the nannofossil assemblages. The Paratethys shared its nannoplankton flora with the world ocean, through ephemeral connections to the Mediterranean. This potentially enables determining the age of Paratethyan sediments with cosmopolitan nannofossil biomarkers until the end of the Miocene (e.g., Marunteanu and Papaianopol, 1998; Mărunţeanu, 1999).

Nannofossil assemblages in the studied samples are moderately to well preserved and typical of the Miocene. Most abundant taxa are *Coccolithus pelagicus* and various *Reticulofenestra* species; *Helicosphaera* spp. are relatively common as well (Fig. 4). Reworked Mesozoic and Paleogene species are present throughout the studied sequence. Their proportion of the assemblage varies but shows a gradual increasing trend from 5 to 25% towards the top of the succession. The LCO of *Cyclicargolithus floridanus* can be observed at 28.7 m; its LO could not be precisely determined as it is obscured by reworking. *Sphenolithus heteromorphus*, the last occurrence of which marks the NN5/NN6 boundary, is not present in the assemblages. The first occurrence of very rare isolated specimens of *Calcidiscus pataecus* (that occurs slightly below the Badenian–Sarmatian boundary) was noted in sample TS23 at 63.8 m, while in sample TS27 at 72.6 m the abundance of the species ephemerally increases to reach about 10% of the entire assemblage. Along with the absence of *Discoaster kugleri*, the marker species of NN7, this suggests that the entire sequence can be assigned to biozone NN6 (Martini, 1971). In the Mediterranean biostratigraphic scheme (Fornaciari et al., 1996) the first common occurrence of *Reticulofenestra pseudoumbilicus* occurs in the lower part of the standard biozone NN6. A distinct rise in abundance of *R. pseudoumbilicus* has been observed in

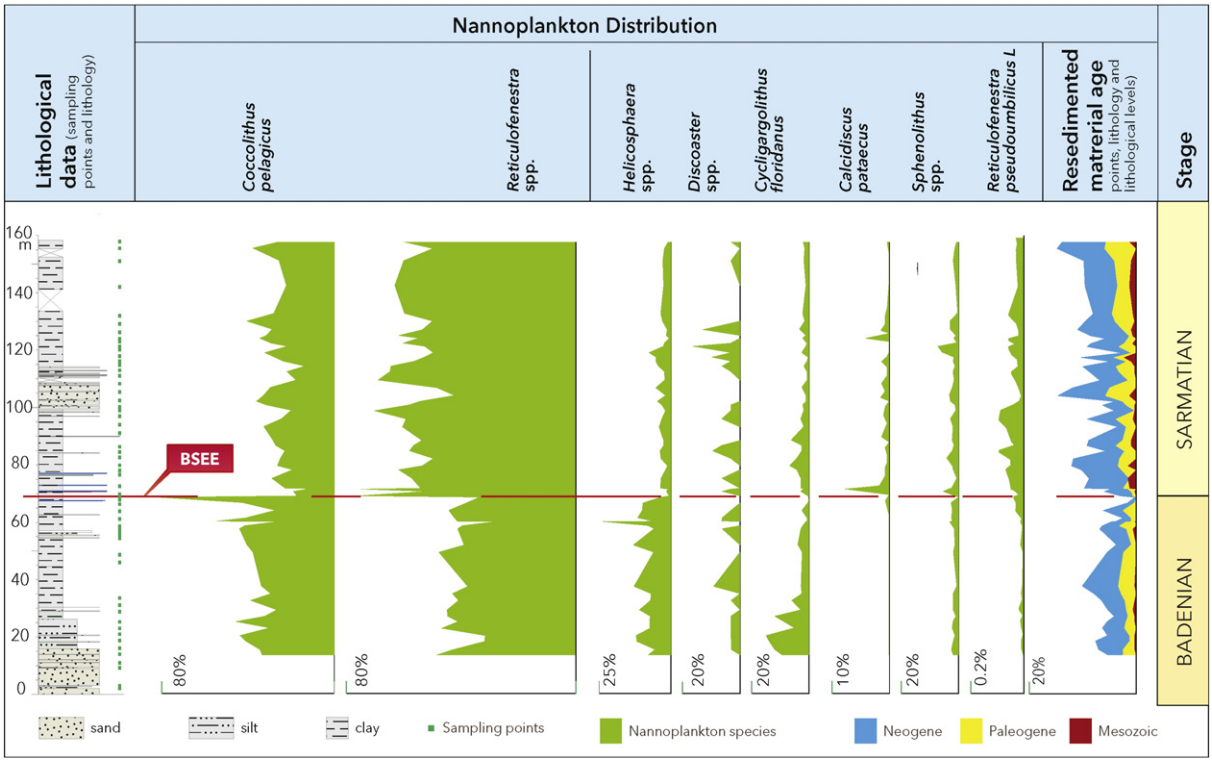

Fig. 4. Quantitative distribution of relevant calcareous nannoplankton taxa against the lithostratigraphy of the Tisa section. Please note differences in scaling. BSEE line indicates the stratigraphic level of the Badenian–Sarmatian Extinction Event.

sample TS23 at 63.8 m in the Tisa section and above, suggesting a correlation to the MNN6a–MNN6b transition. Di Stefano et al. (2008) dated this event in the Mediterranean at 13.1 Ma, yet the timing of this paleoecologically controlled event in the entire Paratethys realm is not necessarily the same (Bartol and H., J, 2015). The major paleoenvironmental changes in this time interval imply that regional depositional conditions may limit such detailed Paratethys–Mediterranean correlations.

3.2.1. The Badenian–Sarmatian boundary interval

A prominent shift of dominance in nannofossil assemblages occurs at the interval identified as the Badenian–Sarmatian boundary. The relative abundance of *C. pelagicus*, the dominant species in the lower part of the section, decreases significantly at the boundary level, while the relative abundance of *Reticulofenestra* spp. increases in the upper part of the section. The *Reticulofenestra* genus is commonly associated with opportunistic behavior (e. g., Krammer et al., 2006); it is able to tolerate a wide range of different nutrient, temperature and salinity levels (e.g., Bartol et al., 2008). In the Tisa section, the rise of *Reticulofenestra* spp. to dominance occurs exactly at the BSEE, coinciding with extinctions of planktonic foraminifera and planktotrophic gastropods (Harzhauser and Piller, 2007) reflecting a severe crisis affecting the plankton. The shifts of dominance between *Reticulofenestra* and *Coccolithus* groups have also been observed in the aftermath of the Miocene Climatic Optimum in the North Atlantic (e.g., Bartol, and H., J, 2015), confirming that *Reticulofenestra* can thrive during times of large-scale climatic deterioration. Our observations confirm that during times of environmental stress *Reticulofenestra* is more successful than *C. pelagicus*. This shifts the focus from climate change to stress, which can be brought on by climate cooling (Bartol, and H., J, 2015), water mass movements (Beaufort and Aubry, 1992) or salinity changes (this manuscript) etc.

The genus *Helicosphaera* has a widespread distribution, but is usually recorded in low abundances in oceanic sediment assemblages and living communities (Baumann et al., 2005). It can be very abundant in Central Paratethys assemblages, where it can occasionally even dominate nannofossil assemblages (Bartol, 2009). The genus is associated with warm surface waters with a medium to high content of nutrients; it is more common in coastal and shelf than pelagic environments (Negri, 2000; Baumann et al., 2005). *Helicosphaera* never dominates the Tisa assemblages. A very distinct drop (~10% to ~2%; Fig. 4) in relative abundance was observed at the Badenian–Sarmatian boundary. A possible explanation for this change in abundance would be a sudden decrease in salinity related to environment deterioration.

3.3. Magnetostratigraphy

We have collected paleomagnetic cores from 95 levels using a handheld electric drill. The orientation of the paleomagnetic cores and the corresponding bedding planes have been obtained using a magnetic compass, previously corrected for the local magnetic declination. In the laboratory rock-magnetic experiments were conducted to understand the nature of the magnetic carrier and afterwards thermal demagnetization technique was applied to isolate the characteristic remanent magnetization (ChRM).

3.3.1. Rock magnetism

Rock-magnetic experiments were carried out on bulk samples in order to identify which are the carriers of the magnetization (magnetic susceptibility, isothermal remanent magnetization (IRM) acquisition, thermomagnetic runs in air).

First, the initial magnetic susceptibility was measured for all samples on a Kappabridge KLY-1. The susceptibility ranges from 2.57E-08 for TS02 to 6.79E-07 for TS87. Plotting the results against the stratigraphic column reveals some particularities (Fig. 6). We can isolate three regions with characteristic magnetic susceptibility behavior: the lower part of the section (0–80 m) is characterized by weak magnetic susceptibility and low variability, the middle part (80–200 m) has stronger magnetic susceptibility and high variability and the upper part (above 200 m) contains the samples with the strongest magnetic susceptibility

and the highest variation. High and low magnetic susceptibility samples from these three regions were selected for Curie Balance analyses.

Thermomagnetic runs were measured in air on a modified horizontal translation type Curie balance with a sensitivity of approximately ~10–9 Am^2 (Mullender et al., 1993). Approximately 40–60 mg of powdered sample was put into a quartz glass sample holder and held in place by quartz wool; heating and cooling rates were 10 °C/min. The thermomagnetic runs show in all cases the alteration of an iron sulfide, transforming above ~400 °C to a more magnetic phase (magnetite) and finally above 580–600 °C, to hematite (Fig. 5).

The samples have variable behavior: most samples show reversible decrease in magnetization up to ~410 °C (Fig. 5 — TS51, TS85), which is characteristic for magnetite with some samples characterized by an irreversible decrease in magnetization with increasing temperature up to ~410 °C which is typical of greigite (Fig. 5, TS81). There are also samples that have mixed characteristics and contain a major reversible component with magnetite properties and a secondary irreversible component with greigite behavior (Fig. 5 — TS09).

3.3.2. Demagnetization results

The natural remanent magnetization (NRM) was thermally demagnetized and measured using a 2G Enterprises DC Squid cryogenic magnetometer (noise level of 3*10–12 Am^2). Heating was applied in a laboratory-built, magnetically shielded furnace, with a residual field less than 10 nT. The heating steps were customized for the samples and ranged between 10 and 40 °C. NRM intensity ranges between 20*10–6 A/m and 71.000*10–4 A/m. Plotting the results against stratigraphic level reveals three intervals:

- The LZ shows low intensities (28.8–362*10–4 A/m) between the base of the section and the ~70 m level;
- The MZ has higher intensities (271*10–4 A/m to 71.169*10–6 A/m) and low frequency of intensity variations between the stratigraphic levels ~70 m and ~200 m;
- The UZ has the highest intensity (41*10–6 A/m to 57.312*10–6 A/m) and high frequency of intensity variations above the stratigraphic level of ~200 m.

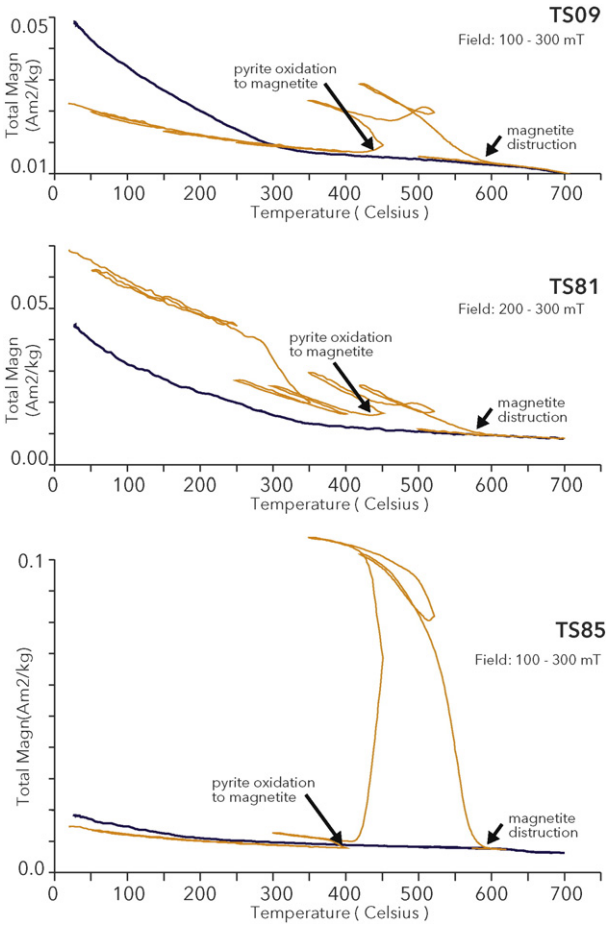

Fig. 5. Thermo-magnetic runs for selected samples. Heating (orange lines) and cooling (dark blue lines) were performed with rates of 10 °C/min. Individual data points have been omitted for clarity. Cycling field varied between 100 and 300 mT for samples TS09 and TS 85 and 200–300 mT for sample TS81. Samples TS09 and TS85 show important alteration after heating above 415 °C probably due to the oxidation of pyrite to magnetite. Sample codes are indicated in the upper right corner.

These three NRM intensity intervals suggest a succession of three different geochemical settings in the basin.

Several characteristic thermal demagnetization diagrams, of mostly marls and clays, are depicted in Fig. 7. We identified the ChRM by analyzing the vector end-point diagrams (Zijderveld, 1967). During progressive stepwise thermal demagnetization two components have been identified. A relatively weak low-temperature, randomly oriented, viscous overprint is generally removed at 120 °C (Fig. 7). A second high-temperature component is demagnetized at temperatures between 120 and 180 °C and 300 °C. This component is of dual polarity and is interpreted as the ChRM. The ChRM directions were defined by at least four consecutive temperature steps and calculated with the use of principal component analysis (Kirschvink, 1980).

The maximum angular deviation (MAD) of the calculated directions has been used to separate the results in four qualitative groups. The 1st quality (MAD = 0–5) and 2nd quality results (MAD = 5–10) have been used for plotting the polarity pattern (Figs. 5 and 7). The 3rd quality results (MAD = 10–15) and 4th quality results (MAD >15) have been plotted as additional points without being taken into account for establishing the polarity pattern (Fig. 5).

The polarity pattern of the Tisa section comprises five different polarity intervals, three of reverse (R1-3) and two of normal (N1-2) polarity. The section starts with reversed polarity interval R1 in which there is a short uncertain interval with two 3rd quality samples of normal polarity. The reversed polarity interval R1 is followed by a short normal interval N1, a longer reversed interval R2, a long normal interval N2 and a reversed interval R3 at the top, where the section ends.

The ChRM directions of the first two groups pass the reversal test of McFadden and McElhinny (1990) at 95% confidence — class B. The normal ChRM directions differ significantly from the present-day field direction (Fig. 8). Our results indicate that the Tisa section experienced a clockwise vertical axis rotation of about 14.5° (Fig. 8), probably related to Miocene tectonic movements during the formation of the Carpathians (Dupont-Nivet et al., 2005; De Leeuw et al., 2013).

4. Chronologic framework for the BSEE

With the help of integrated stratigraphy we can provide an age for the BSEE. Foraminiferal and nannoplankton data are used to identify and locate the extinction event in the Tisa section and to provide supplementary information on the environmental changes in the basin. Magnetostratigraphy will give the age by correlation to the geologic polarity time scale (Hilgen et al., 2012). This approach has earlier been proven successful in Central Paratethys sediments if sections are well-tuned to the nature of the magnetic carriers (Vasiliev et al., 2007; Paulissen et al., 2011; De Leeuw et al., 2013; ter Borgh et al., 2013).

We plotted the ChRM directions, magnetic intensity and magnetic susceptibility against stratigraphic level (Fig. 6) to compare our paleomagnetic polarity pattern with the biostratigraphic results. By matching the observed polarity pattern of the Tisa section with the geomagnetic polarity time scale (GPTS) (Hilgen et al., 2012) we can place the section and the BSEE event in a robust time frame (Fig. 9). This allows us to calculate the age of the BSEE.

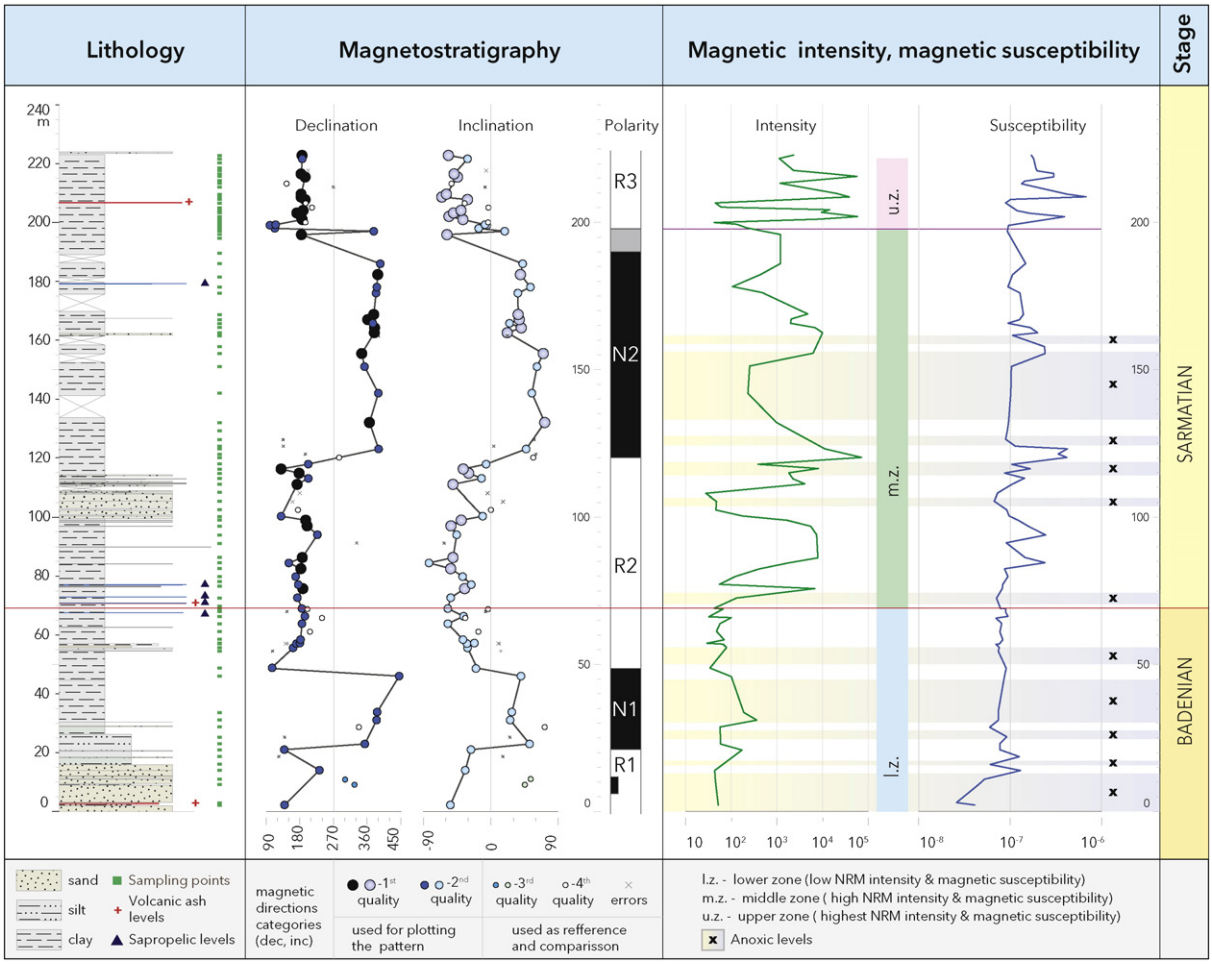

Fig. 6. Schematic lithological column, polarity zones, magnetic intensity and magnetic susceptibility for the Tisa section. Three reversed polarity intervals (R1, R2, R3) and two normal ones (N1, N2) have been identified. The position of the BSEE is marked with a red line. Note the change in the magnetic intensity and susceptibility, both measured at 20 °C, that occurs across the boundary.

The best-fit correlation of the Tisa polarity pattern is with the chron succession C5Ar.2r–C5An.1r (Fig. 10). In fact, this is the only interval in the NN6 range (13.53–11.90 Ma) where the pattern: short normal/long reversed/long normal is observed. This indicates that the Tisa section comprises the time interval between 12.8 and 12.2 Ma, roughly corresponding to the middle Serravallian (Fig. 10).

Our biostratigraphic data shows that the BSEE is located between the sampling points TS25 and TS26 (Figs. 4 and 6), corresponding to an average stratigraphic level of 68.4 m (between 67.8 and 69 m). This level also corresponds with the LZ–MZ boundary in the magnetic proxy records, which suggests that the BSEE had a component of environmental change that significantly affected the magnetic properties of the sediments in the basin. Correlated with the paleomagnetic polarity patterns the BSEE is located in the lower half of the reversed interval R2 and corresponds to Chron C5Ar.1r (12.735 to 12.474 Ma) (Fig. 9). Based on the hypothesis of a constant sedimentation rate (0.27 m/kyr) throughout the C5Ar.1r Chron, this provides an age of **12**.66 Ma for the BSEE.

To evaluate this age value we also test the hypothesis of a variable sedimentation rates throughout the section, based on the grain size of the sediments. The interval that corresponds to C5Ar.1r predominantly consists of marls, except the top part where 20 m thick sand layers are present. These sand layers most likely correspond to higher sedimentation rates, but the exact rates cannot be calculated. Assuming similar high sedimentation rates of 0.72 m/kyr as in the sand-rich base of the section, we obtain an age of 12.64 Ma for the BSEE event. By averaging this age model with the previous one we date the BSEE at 12.65 ± 0.01 Ma.

5. Discussion

5.1. Paleoenvironmental changes at the BSEE

The Badenian sediments in the section (level 0–68.4 m) reveal a highly restricted environment with deteriorated, poorly oxygenated bottom conditions in the basin, including several short intervals of anoxia (Fig. 3). *C. pelagicus* is the dominant nannofossil species and the foraminifera assemblages contain taxa that are confined to normal marine salinity. Just prior to the BSEE (57.7–68.4 m), environmental conditions tend to improve and the diversity of the benthic foraminifera increases from 2 to 9 species (Fig. 3).

In the Sarmatian part of the section (68.4–132 m) the planktic foraminifera have fully disappeared while a new benthic fauna progressively develops, fragmented again by barren intervals related to anoxic episodes. Anoxia episodes persist throughout the entire section and show no direct relation with the extinction event. The Sarmatian benthic foraminifera species are characteristic for brackish conditions indicating that water chemistry changes play a significant role at the extinction of the Badenian taxa. The nannoplankton species distribution also changed across the BSEE, with relative abundance of *Reticulofenestra* spp. and that of *C. pelagicus* decreasing. This shift is interpreted to relate to increasing environmental stress in the basin, probably also related to a sudden decrease in salinity.

The upper Badenian-lower Sarmatian lithological succession of the Carpathian foredeep sections generally shows fining-up features. There is no evidence for sea level change at or close to the BSEE. The

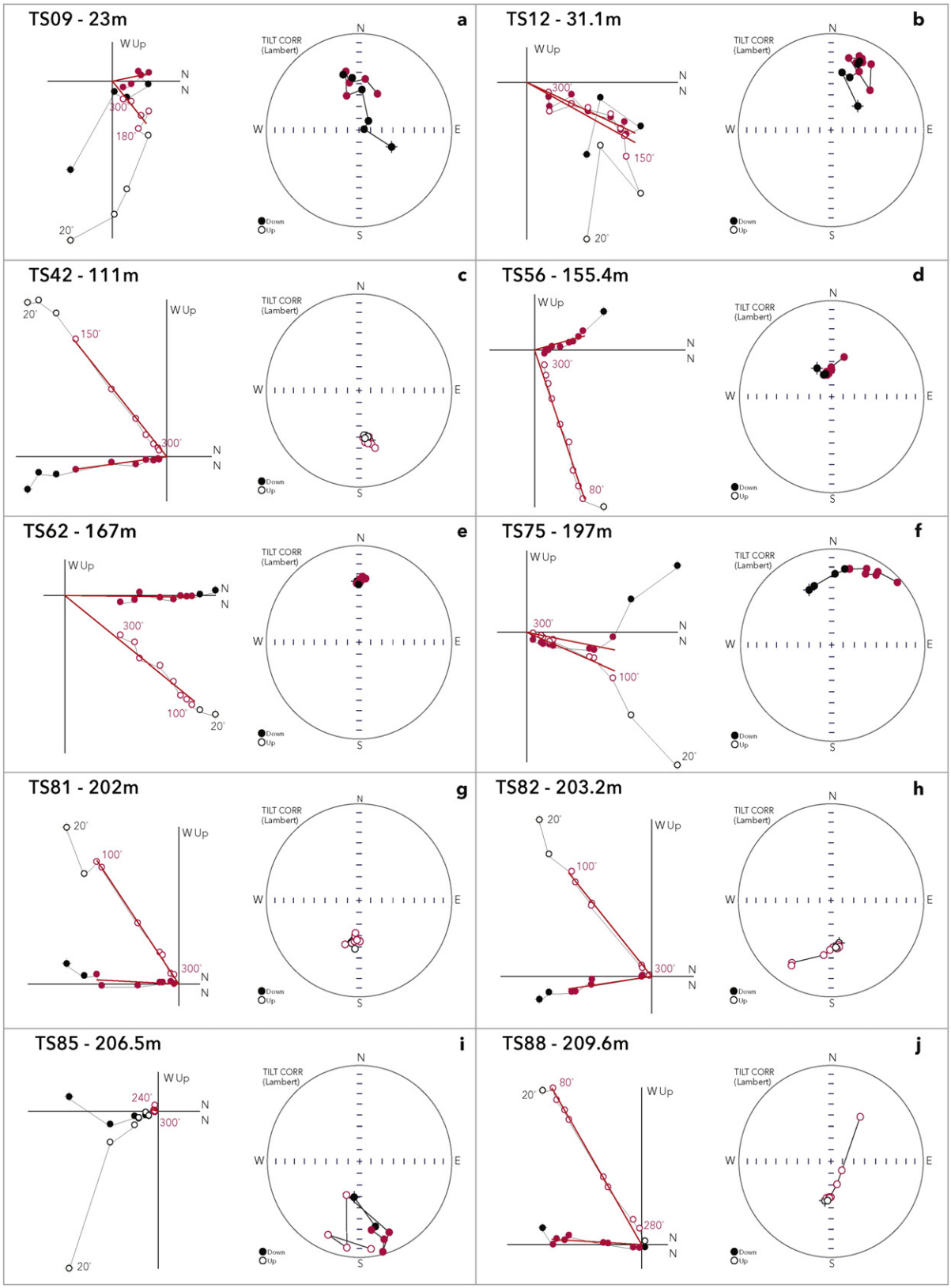

Fig. 7. Representative examples of Zijderveld demagnetization diagrams and Equal Area projections after tilt correction. Sample code and stratigraphic level are specified in the upper left corner. Solid (open) circles represent the projection on the horizontal (vertical) plane. The numbers represent the subsequent demagnetization steps in degrees Celsius. The red dots (numbers) represent the points used for calculating the ChRM component which is marked by the red lines.

coarser sand-rich upper Badenian sediments from the base of the Tisa section, ~70 m below the boundary, could be indicative for a low-stand but they could also be result of local tectonic events. The Badenian species *Q. regularis* as well as the Sarmatian markers *C. stomata* and *V. reussi* are all indicative of deep basinal settings (Łuczkowska, 1974) suggesting that sea level change is not a dominant factor at the BSEE.

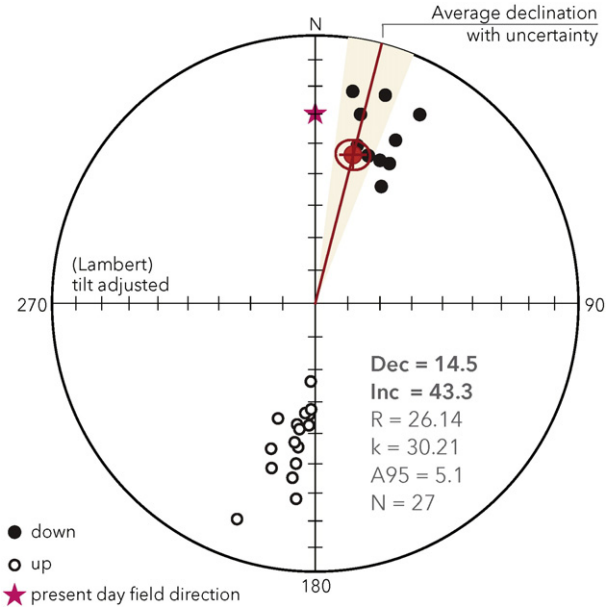

Fig. 8. Stereographic plot of the ChRM directions of the Tisa section, tilt correction applied. Normal (reversed) measurements are plotted with closed (open) symbols. The red line indicates the average declination and the gray area the corresponding uncertainty (dDx).

The most striking feature of the BSEE in the Tisa section is the sudden, sharp disappearance of Badenian fauna. The extinction of Badenian taxa occurs in a 1.2 m thick interval, equivalent to less than 10 kyr (value calculated using the average sedimentation (Fig. **9**). We conclude that the extinction of the open marine Badenian taxa is directly linked with an extremely rapid change of salinity within the basin.

5.2. The BSEE in the Central Paratethys

Our results show that a major and rapid paleoenvironmental change took place at 12.65 ± 0.01 Ma correlative to the BSEE in the Romanian Carpathian foredeep. Regarding the paleogeographic context of Central Paratethys, being characterized by mostly fragmented basins, it is important to understand if the BSEE event occurred diachronously in different basins or synchronously throughout the entire Paratethys domain. Consequently, we compare our results to previous magnetostratigraphic dating attempts in the other sub-basins of Central Paratethys: e.g. the Vienna Basin, Pannonian Basin and Transylvanian Basin (Fig. 1).

In the most recent time scales for the Central Paratethys the Badenian–Sarmatian boundary is placed at 12.7 Ma (Piller et al., 2007; Hilgen et al., 2012), in good agreement with our new age determination. This boundary is inferred to correspond to a Paratethys-wide turnover in faunal elements, triggered by strong restriction of the connections to the open ocean. In several basins the boundary interval corresponds to an erosive discordance, which restricts more accurate age determinations (Harzhauser and Piller, 2004).

In the Vienna Basin, the Badenian–Sarmatian boundary has been penetrated in several wells, but microfaunal contamination generally hampers a precise determination of the stratigraphic horizon (Harzhauser and Piller, 2004). Paulissen et al. (2011) attempted to date the B–S boundary in the Spannberg-21 well using an integrated paleomagnetic and biostratigraphic approach. Here, the Badenian–Sarmatian boundary interval is slightly disturbed by an erosional surface and influenced by reworking of microfossils. The paleomagnetic record of the Badenian part of the well is especially difficult to interpret because of weak magnetic signals (Paulissen et al., 2011). Despite these uncertainties, a correlation could be established to the C5Ar.1r chron, in agreement with our results from the Carpathian foredeep. Hohenegger et al. (2014) recently suggested placing the boundary at the top of

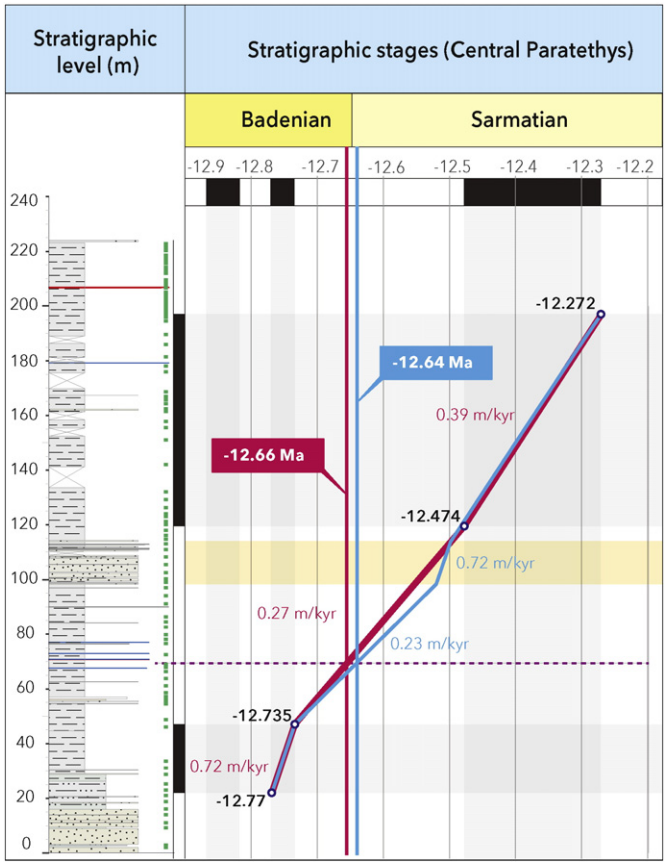

Fig. 9. Age model for the BSEE of the Tisa section. The dotted purple line represents the BSEE. The gray bands represent the normal polarity intervals and the yellow band marks the sandy interval. Two calculation scenarios were used: a. constant sedimentation throughout the sandy interval (red), b. variable sedimentation in the sandy interval (blue).

polarity chron C5Ar.2r at an age of 12.829 Ma, but this correlation was not based on any paleomagnetic data.

In the Pannonian basin, Selmeczi et al. (2012) carried out magnetostratigraphic and paleontological studies on the Badenian–Sarmatian succession in the borehole Nagylózs-1 in Hungary. They correlated the B–S boundary to chron C5AAn and a corresponding age of 13.15 Ma, but the polarity pattern of this borehole is not straightforward and correlations to younger intervals cannot be excluded. A magnetostratigraphic study on Badenian–Sarmatian drill cores from the North Carpathian foredeep basin in Poland was hampered by a pervasive paleomagnetic overprint related to late diagenetic growth of greigite (Sant, 2015). De Leeuw et al. (2013) combined magnetostratigraphic, biostratigraphic and Ar/Ar data from multiple sections and outcrops in the Transylvanian Basin, and interpolated the age of the Badenian–Sarmatian boundary, based on the assumption of constant sedimentation rate, between 12.7 and 12.83 Ma. The high uncertainty is mainly related to the presence of large gaps in the composite magnetostratigraphic record. We conclude that these results are not necessarily in disagreement with our new age model.

Our new age of 12.65 ± 0.01 Ma is in relatively good agreement with many other records from different Paratethys basins, which suggests that the BSEE is likely a synchronous event over the entire Central Paratethys. We see no sufficiently strong argument in the present data sets to infer a diachrony in paleoenvironmental change affecting the various sub-basins.

5.3. Correlations to the Eastern Paratethys

In the Eastern Paratethys, the uppermost Badenian is generally correlated to the Konkian stage (Rögl, 1998; Studencka et al., 1998). The

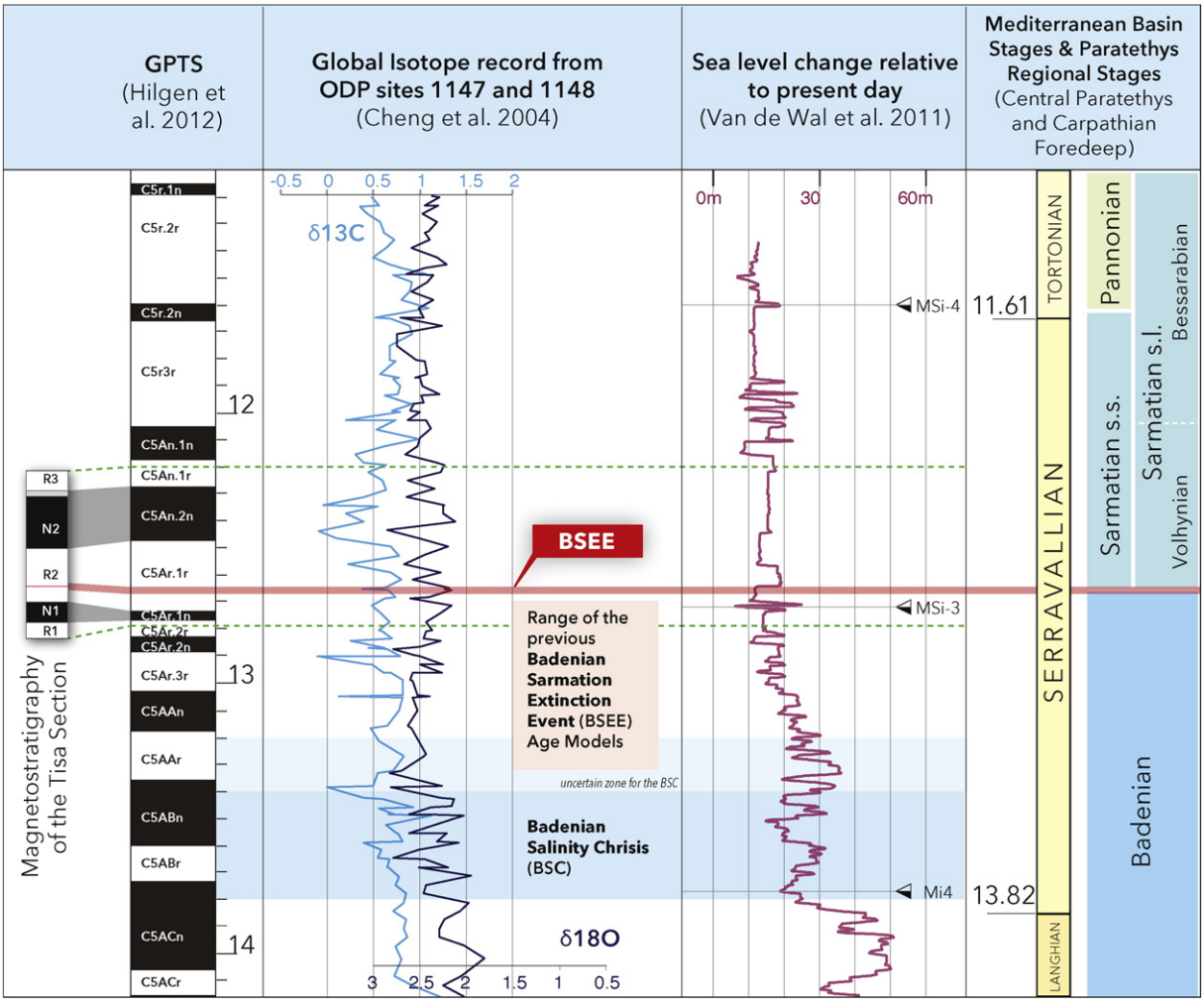

Fig. 10. Correlation of the polarity sequence of the Tisa section with the GPTS, the global oxygen and carbon isotope records and the sea-level fluctuations. The gray bands correlate the polarity pattern of the section with the GPTS. Note that this is the only logical correlation of the short normal-long reverse-long normal pattern of the Tisa section in the relevant time interval. The green dashed lines are the estimated range of the Tisa section. The red line represents the BSEE. Note that it does not correlate with any major C or O event in the isotope records. The BSEE matches a small sea-level rise at 12.64 Ma.

Konkian is followed by the Sarmatian and the Konkian–Sarmatian boundary is considered equivalent of the Badenian–Sarmatian boundary (Studencka and Jasionowski, 2011). The exact nature of the Konkian–Volhynian boundary is controversial and there is no direct evidence for a major extinction event, at this time, in Eastern Paratethys. The Konkian mollusks are identified as ancestors of the Volhynian taxa (Studencka et al., 1998) which suggests that a less dramatic faunal change in the occurred in Eastern Paratethys in the form of a development of the already endemic brackish Konkian mollusks faunas. No reliable age determinations exist to date the Konkian–Volhynian boundary (e.g. Popov et al., 2006), which makes any high-resolution correlations difficult.

5.4. The BSEE and global change

The Badenian–Sarmatian boundary has previously been correlated to sequence stratigraphic frameworks (Fig. 10), where it corresponds to the Ser3 sequence of Hardenbol et al. (1998). This sequence is in turn correlated to the glacio-eustatic lowstand TB 2.6 (Haq et al., 1988) and MSi-3 (Abreu and Haddad, 1998). In contrast, the recently established sea-level curve (Van De Wal et al., 2011) does not reveal any significant sea level lowstands in the 13–12 Ma time interval. Instead, the BSEE event seems to correlate with a ~10 m sea level rise, which is dated at 12.64 Ma. In addition, the stable oxygen and carbon isotope curves (Holbourn et al., 2005; Cheng et al., 2004) also do not show any significant event at the age of 12.65, suggesting that global climate change did not play a major role in the paleoenvironmental changes triggering the BSEE.

5.5. Paleogeographic changes at the BSEE

During the middle Badenian, the only marine connection of the Central Paratethys was with the Mediterranean through the Slovenian strait or Trans-Tethyan Corridor (Fig. 11). The exact age of the Slovenian gateway closure remains uncertain but recent studies indicate that it may well have been open, although very restrictive, during the late Badenian-early Sarmatian (Bartol et al., 2014). The marine Central Paratethys became connected with the brackish Eastern Paratethys realm in late Badenian/Konkian times through opening of the Barlad Strait (Fig. 11a; Popov et al., 2004). The existence of this connection is evidenced by one-way faunal migrations in the late Badenian from Central towards Eastern Paratethys (Studencka et al., 1998), probably due to different salinity regimes in the two domains. Towards the end of the Badenian the gateway became ineffective leading to the loss of all euryhaline taxa in the Eastern Paratethys (Vernigorova, 2009). The Barlad gateway developed into a wide, open sea corridor at the beginning of the Sarmatian (Volhynian) (Pevzner, and V, E.A, 1993) (Fig. 11b). The two-Paratethyan realms were joined to form a single

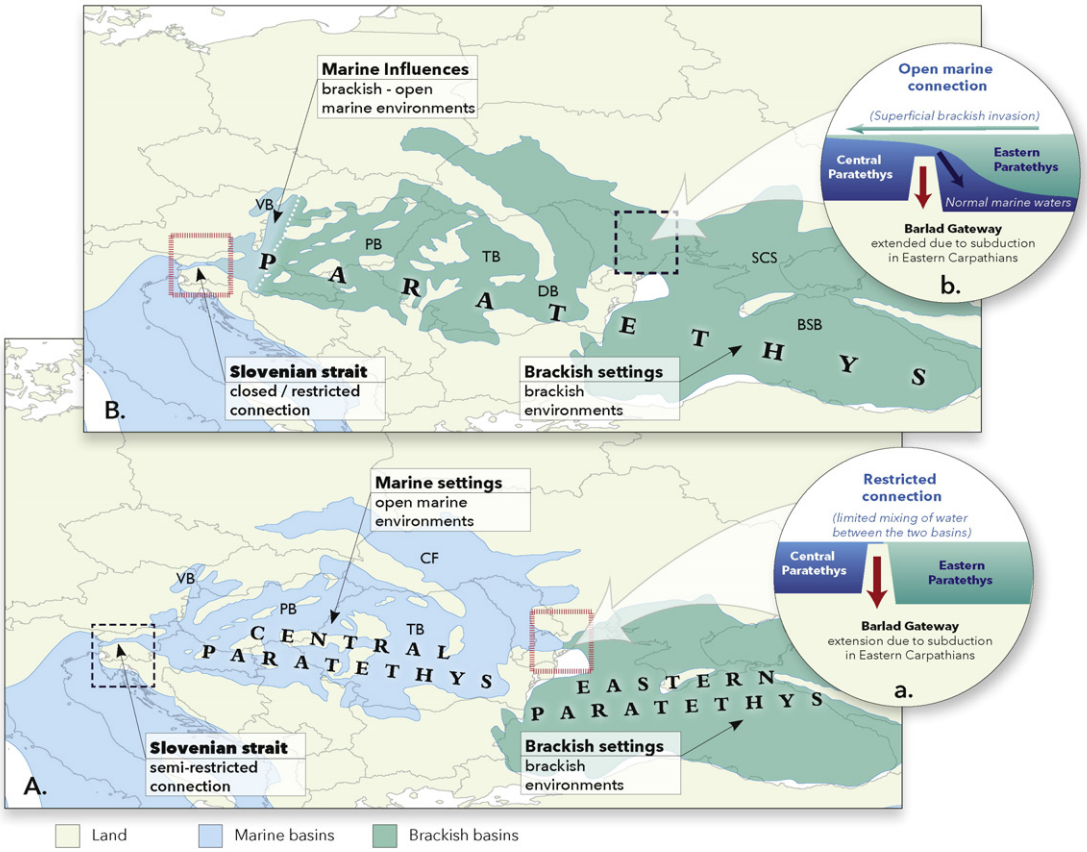

Fig. 11. The evolution of gateways and the change in salinity at the end of the Middle Miocene in Central and Eastern Paratethys basins (modified after Popov et al., 2004, Kojumdgieva, 1983 and Pevzner, and V, E.A, 1993). (A) Paleogeographic setting during the latest Badenian (Serravallian ~12.65 Ma). At this time the connection between Eastern and Central Paratethys through the Barlad Strait (inset (a.)) was restricted, allowing only limited exchange of water, resembling the present day Bosphorus Strait. (B) Paleogeographic setting during the early Sarmatian–Volhynian substage (Late Serravallian–Early Tortonian, after 12.65 Ma). The Barlad Strait widens and deepens (inset (b.)), becoming a full marine connection and allowing a stratified water exchange. Abbreviations for the relevant Paratethys sub-basins: BSB — Black Sea Basin, CF — Carpathian Foredeep, PB — Pannonian Basin, SCS — Scythian Shelf, TB — Transylvanian Basin, VB — Vienna Basin, and DB — Dacian Basin.

united Paratethys Sea (Fig. 11b). This Volhynian sea had a strikingly uniform, endemic "Sarmatian" fauna (Studencka et al., 1998), indicating an effective water exchange between the basins. The BSEE thus corresponds with a major transformation in the nature of the Barlad gateway, switching from a passive to a full connection between Central and Eastern Paratethys.

The widening and deepening of the Barlad gateway was most likely triggered by tectonics. The area is part of the Eastern European plate that was subsiding under the Tisza–Dacia plate during the Badenian and Sarmatian times (Matenco et al., 2010). Seismic data from the Carpathian Foredeep basin show a depocenter change at the BSEE level, which can also be related to the tectonic reorganizations in the region (Tarapoanca et al., 2003).

In addition, the global sea level rise, taking place at 12.64 Ma (Van De Wal et al., 2011), would clearly help to increase the water exchange between the two Paratethys domains. Arguments for such a transgressive event are found in many Paratethyan basins (Kováč et al., 2004; Kováč et al., 2007; Filipescu and De Leeuw, 2011) where the earliest Sarmatian deposits are extended on a larger surface than the latest Badenian sediments. The significantly smaller Central Paratethys clearly experienced a far more drastic change in water chemistry than the large Eastern Paratethys basin. Our results indicate that this change in chemistry is exemplified by a change from marine to brackish conditions in the Central Paratethys and that it took place at 12.65 ± 0.01 Ma in a very short time interval of less than 10 kyr. The Slovenian gateway probably still allowed restrictive Paratethys–Mediterranean exchange during the early Sarmatian, generating more saline influxes in especially the westernmost part of Paratethys (Piller and Harzhauser, 2005).

6. Conclusions

We provide integrated magneto-biostratigraphic results for a continuous, 220 m long, sedimentary succession in the Carpathian foredeep basin of Romania that straddles the Badenian–Sarmatian boundary interval. All marine Badenian species suddenly disappear in a very short stratigraphic interval between 67.8 and 69.0 m, correlative to the BSEE. Quantitative micropaleontological analyses of foraminifera and calcareous nannofossils reveal that the BSEE in the Tisa section corresponds to a rapid change in basin chemistry, with open marine conditions changing to brackish water environments. The magnetostratigraphic record from the section can be straightforwardly correlated to the GPTS, and shows that it covers the time interval from 12.8 to 12.2 Ma. The Badenian–Sarmatian boundary is located in the lower half of chron C5Ar.1r corresponding to an age of 12.65 ± 0.01 Ma, in good agreement with earlier results (Piller et al., 2007; Paulissen et al., 2011; De Leeuw et al., 2013). We furthermore conclude that the BSEE happened very fast, in a time span of less than 10 kyr.

We found no evidence for a sea-level drop at the BSEE level or for a major change in global climate. Paleogeographic reconstructions show that the BSEE does correspond to a change in the configuration of the Central–Eastern Paratethys gateway: the so-called Barlad Strait (Popov et al., 2004) and a minor rise in global sea level (Van De Wal et al., 2011). It suggests that the marine Central Paratethys became fully connected with the predominantly brackish Eastern Paratethys, resulting in a unified Paratethys sea at the beginning of the Sarmatian, causing a dramatic change towards less saline conditions in the Central Paratethyan basins. A small, restricted marine connection with the

Mediterranean probably persisted during the early Sarmatian, allowing for more saline conditions in the westernmost part of Paratethys (Piller and Harzhauser, 2005).

Acknowledgments

Special thanks go to Charon Duermeijer, Savi and Kyro for discovering the Tisa section with us. Georghe Popescu, Monica Crihan and Marius Stoica are thanked for their guidance with the biostratigraphic analyses. Karin Sant, Andrei Strachinaru, Ioana Novac, Daniel Stefan, Florian Bolbocean, Catalin Dumitrache, Sergiu Badianu, Cola Draghici and Izabela Maris are thanked for helping with the sampling the section. Special thanks to Constantin Dobre, the local forestry manager for gracefully granting us full support to access the section. Marius Stoica and Sergey Popov are acknowledged for detailed and constructive discussions. This work was financially supported by the Netherlands Geosciences Foundation (ALW) with support from the Netherlands Organization for Scientific Research (NWO) through the VICI grant of WK.

References

Abreu, V.S., Haddad, G.A., 1998. Glacioeustatic fluctuations: the mechanism linking stable isotope events and sequence stratigraphy from the early Oligocene to middle Miocene. Mesozoic Cenozoic Sequence Stratigr. Eur. Basins 60, 245–259.

Bartol, M., 2009. Middle Miocene calcareous nannoplankton of NE Slovenia (western Central Paratethys). Založba ZRC 2009.

Bartol, M., et al., 2014. Paleontological evidence of communication between the Central Paratethys and the Mediterranean in the late Badenian/early Serravallian. Palaeogeogr. Palaeoclimatol. Palaeoecol. 394, 144–157.

Bartol, M., et al., 2008. Unusual *Braarudosphaera bigelowii* and *Micrantholithus vesper* enrichment in the Early Miocene sediments from the Slovenian Corridor, a seaway linking the Central Paratethys and the Mediterranean. Palaeogeogr. Palaeoclimatol. Palaeoecol. 267 (1–2), 77–88.

Bartol, M., H., J, 2015. Nannofossil assemblage shifts in the aftermath of the Miocene Climatic Optimum — a North Atlantic latitudinal transect - March 7–16, 2015. INA15 Abstract Volume.

Baumann, K.H., Andruleit, H., Geisen, M., Kinkel, A., 2005. The significance of extant coccolithophores as indicators of ocean water masses, surface water temperature, and paleoproductivity: a review. Paläontol. Z. 79, 93–112.

Beaufort, L., Aubry, M.-P., 1992. Occurrence and stratigraphy of *Coccolithus pelagicus* in ODP Hole 120-747A. doi:10.1594/PANGAEA.758888, *Supplement* to: Beaufort, L. and Aubry, M-P. (1992): paleoceanographic implications of a 17-m.y.-long record of high-latitude Miocene calcareous nannoplankton fluctuations. Proc. Ocean Drill. Program Sci. Results, Coll. Station, TX (Ocean Drilling Program) 120, 539–549.

Cheng, X., et al., 2004. Data report: stable isotopes from Sites 1147 and 1148. In: Prell, W.L., Wang, P., Blum, P., Rea, D.K., Clemens, S.C. (Eds.), Proc. ODP, Sci. Results. College Station, TX (Ocean Drilling Program), pp. 1–12.

Crihan, I., 1999. Studiul Lito-Biostratigrafic al Miocenului Mediu Dintre Valea Prahovei si Valea Teleajanului, la Sud de Sinclinalul Slanic (Unpublished PhD thesis, Cluj-Napoca).

Crihan, I., 2002. Sarmatian foraminifera assemblages from the Melicesti syncline (Subcarpathians of Muntenia) and their paleoecological significance. A case study. Stud. Univ. Babes-Bolyai, Geol., Spec. Issue 1, 153–164.

Cicha, I., Seneš, J., 1968. Sur la position du Miocene de la Paratcthys Central dans les cadre du Tertiaire de l'Europe. Geol. Sb. 19 (1), 95–116.

De Leeuw, A., et al., 2013. Paleomagnetic and chronostratigraphic constraints on the middle to late Miocene evolution of the Transylvanian basin (Romania): implications for Central Paratethys stratigraphy and emplacement of the Tisza–Dacia plate. Glob. Planet. Chang. 103 (1), 82–98.

Di Stefano, A., et al., 2008. Calcareous plankton high resolution bio-magnetostratigraphy for the Langhian of the Mediterranean area. Riv. Ital. Paleontol. Stratigr. 114 (1), 51–76.

Dumitrica, P., et al., 1975. New data on the biostratigraphy and correlation of the Middle Miocene in the Carpathian area. Dari De Seama Ale Sedintelor 61 (4), 65–84.

Dupont-Nivet, G., et al., 2005. Neogene tectonic evolution of the southern and eastern Carpathians constrained by paleomagnetism. Earth Planet. Sci. Lett. 236 (1–2), 374–387.

Filipescu, S., De Leeuw, A., 2011. Calibration of several foraminifera biozones in the marine Miocene from Romania. The 4th International Workshop on the Neogene from the Central and South-Eastern Europe. Abstracts and Guide of Excursion, pp. 28–29.

Fornaciari, E., et al., 1996. Middle Miocene quantitative calcareous nannofossil biostratigraphy in the Mediterranean region. Micropaleontology 42 (1), 37–63.

Haq, B.U., et al., 1988. Mesozoic and Cenozoic chronostratigraphy and cycles of sea-level change. Sea-level changes: an integrated approach, pp. 71–108.

Hardenbol, J., et al., 1998. Mesozoic and Cenozoic sequence chronostratigraphic framework of European basins. Mesozoic and Cenozoic Sequence Stratigraphy of European Basins 60, pp. 3–13.

Harzhauser, M., Piller, W.E., 2004. Integrated stratigraphy of the Sarmatian (Upper Middle Miocene) in the western Central Paratethys. Stratigraphy 1 (1), 65–86.

Harzhauser, M., Piller, W.E., 2007. Benchmark data of a changing sea — palaeogeography, palaeobiogeography and events in the Central Paratethys during the Miocene. Palaeogeogr. Palaeoclimatol. Palaeoecol. 253 (1–2), 8–31.

Hilgen, F.J., et al., 2012. (2012). the Neogene period. Geol. Time Scale 1–2, 923–978.

Hohenegger, J., et al., 2009a. The Styrian Basin: a key to the Middle Miocene (Badenian/Langhian) Central Paratethys transgressions. Aust. J. Earth Sci. 102 (1), 102–132.

Hohenegger, J., et al., 2009b. Cyclostratigraphic dating in the Lower Badenian (Middle Miocene) of the Vienna Basin (Austria): The Baden-Sooss core. Int. J. Earth Sci. 98 (4), 915–930.

Hohenegger, J., et al., 2014. Timing of the middle miocene badenian stage of the Central Paratethys. Geol. Carpath. 65 (1), 55–66.

Holbourn, A., et al., 2005. Impacts of orbital forcing and atmospheric carbon dioxide on Miocene ice-sheet expansion. Nature 438 (7067), 483–487.

Kirschvink, J.L., 1980. The least-squares line and plane and the analysis of palaeomagnetic data. Geophys. J. R. Astron. Soc. 62 (3), 699–718.

Kojumdgieva, E., 1983. Palaeogeographic environment during the desiccation of the Black Sea. –. Palaeogeogr. Palaeoclimatol. Palaeoecol. 43, 195–204.

Kováč, M., et al., 2007. Badenian evolution of the Central Paratethys Sea: paleogeography, climate and eustatic sea-level changes. Geol. Carpath. 58 (6), 579–606.

Kováč, M., et al., 2004. Miocene depositional systems and sequence stratigraphy of the Vienna Basin. CFS Courier Forschungsinstitut Senckenberg, pp. 187–212.

Krammer, R., Baumann, K.H., Henrich, R., 2006. Middle to late Miocene fluctuations in the incipient Benguela Upwelling System revealed by calcareous nannofossil assemblages (ODP Site 1085A). Palaeogeogr. Palaeoclimatol. Palaeoecol. 230, 319–334.

Krijgsman, W., et al., 2010. Rise and fall of the Paratethys Sea during the Messinian Salinity Crisis. Earth Planet. Sci. Lett. 290 (1–2), 183–191.

Laskarev, V., 1924. Sur les equivalentes du Sarmatien supérieur en Serbie. Recueil de traveaux ofert a M. Jovan Cvijic par ses amis et collaborateurs:, pp. 73–85.

Lirer, F., et al., 2009. Astronomically forced teleconnection between Paratethyan and Mediterranean sediments during the Middle and Late Miocene. Palaeogeogr. Palaeoclimatol. Palaeoecol. 275 (1–4), 1–13.

Łuczkowska, E., 1974. Miliolidae (Foraminiferida) from Miocene of Poland. Part II. Biostratigraphy, palaeoecology and systematics. Acta Palaeontol. Pol. 19 (1), 1–176.

Martini, E., 1971. Standard tertiary and quaternary calcareous nannoplankton zonation. Proc. Second Planktonic Conf. 2, 739–785.

Mărunţeanu, M., 1999. Litho and biostratigraphy (calcareous nannoplankton) of the Miocene deposits from the Outer Moldavides. Geol. Carpath. 50 (4), 313–324.

Marunteanu, M., Papaianopol, I., 1998. Mediterranean calcareous nannoplankton in the Dacic Basin. Rom. J. Stratigr. 78, 115–121.

Matenco, L., et al., 2010. Characteristics of collisional orogens with low topographic build-up: an example from the Carpathians. Terra Nova 22 (3), 155–165.

McFadden, P.L., McElhinny, M.W., 1990. Classification of the reversal test in palaeomagnetism. Geophys. J. Int. 103 (3), 725–729.

Mullender, T.A.T., Van Velzen, A.J., Dekkers, M.J., 1993. Continuous drift correction and separate identification of ferromagnetic and paramagnetic contribution in thermomagnetic runs. Geophys. J. Int. 114, 663–672.

Negri, A.V.G., 2000. Calcareous nannofossil biostratigraphy, biochronology and paleoecology at the Tortonian/Messinian boundary of the Faneromeni section (Crete. Palaeogeogr. Palaeoclimatol. Palaeoecol. 156, 195–209.

Papp, A., et al., 1968. Zur Nomenklatur des Neogens in Österreich. Verh. Geol. Bundesanst. 1968, 9–27.

Paulissen, W., et al., 2011. Integrated high-resolution stratigraphy of a Middle to Late Miocene sedimentary sequence in the central part of the Vienna Basin. Geol. Carpath. 62 (2), 155–169.

Pevzner, M.A., V, E.A, 1993. Magnetochronological age assignments of Middle and Late Sarmatian Mammalian localities of the Eastern Paratethys. Newsl. Stratigr. 29, 63–75.

Piller, W.E., Harzhauser, M., 2005. The myth of the brackish Sarmatian Sea. Terra Nova 17 (5), 450–455.

Piller, W.E., et al., 2007. Miocene Central Paratethys stratigraphy — current status and future directions. Stratigraphy 4 (2–3), 151–168.

Popescu, G., 1979. Kossovian Foraminifera in Romania. Geological and Geophysical Institute, Memoire vol. XXIX, Project 25: Stratigraphic Correlation of the Tethys–Paratethys Neogene: 5–110.

Popescu, G., 1995. Contribution of the Sarmatian foraminifera of Romania. Rom. J. Paleontol. 76, 85–98 (Bucuresti).

Popescu, G., 1999. Lower and Middle Miocene agglutinated foraminifera from the Carpathian area. Acta Palaeontol. Rom. 2, 407–425.

Popescu, G., Crihan, I.-M., 2011. Middle Miocene Globigerinas of Romania. Acta Palaeontol. Rom. 7, 291–313.

Popov, S.V., et al., 2004. Lithological–paleogeographic maps of Paratethys. CFS Courier Forschungsinstitut Senckenberg, pp. 1–46.

Popov, S.V., et al., 2006. Late Miocene to Pliocene palaeogeography of the Paratethys and its relation to the Mediterranean. Palaeogeogr. Palaeoclimatol. Palaeoecol. 238 (1–4), 91–106.

Popov, S.V., et al., 2013. Eastern Paratethys stratigraphic scale of Neogene: correlation possibilities. Abstr. 14th RCMNS congress, 8–12 September 2013, Istanbul (Turkey).

Reichenbacher, B., et al., 2013. A new magnetostratigraphic framework for the Lower Miocene (Burdigalian/Ottnangian, Karpatian) in the North Alpine Foreland Basin. Swiss J. Geosci. 106 (2), 309–334.

Rögl, F., 1998. Palaeogeographic considerations for Mediterranean and Paratethys seaways (Oligocene to Miocene). Ann. Naturhist. Mus. Wien **99 A**(A), 279–310.

Sant, K., 2015. Paleomagnetic analyses on Badenian–Sarmatian drill cores from the North Carpathian Foredeep (Middle Miocene, Poland). Biuletyn Państwowego Instytutu Geologicznego 461, 179–192.

Selmeczi, I., et al., 2012. Correlation of bio-and magnetostratigraphy of Badenian sequences from western and northern Hungary. Geol. Carpath. 63 (3), 219–232.

Senes, J., 1961. Paläogeographie des Westkarpatischen Raumes in Beziehung zur übrigen Paratethys im Miozän. Geol. Práce 60, 1–56.
Śliwiński, M., 2012. Badenian–Sarmatian chronostratigraphy in the Polish Carpathian Foredeep. Palaeogeogr. Palaeoclimatol. Palaeoecol. 326–328, 12–29.
Studencka, B., et al., 1998. The bivalve faunas as a basis for reconstruction of the Middle Miocene history of the Paratethys. Acta Geol. Pol. 48 (3), 285–342.
Studencka, B., Jasionowski, M., 2011. Bivalves from the Middle Miocene reefs of Poland and Ukraine: a new approach to Badenian/Sarmatian boundary in the Paratethys. Acta Geol. Pol. 61, 79–114.
Tarapoanca, M., et al., 2003. Architecture of the Focşani Depression: a 13 km deep basin in the Carpathians bend zone (Romania). Tectonics 22 (6), 13-11–13-18.
ter Borgh, M., et al., 2013. The isolation of the Pannonian basin (Central Paratethys): new constraints from magnetostratigraphy and biostratigraphy. Glob. Planet. Chang. 103 (1), 99–118.
Van Baak, C.G.C., et al., 2013. A magnetostratigraphic time frame for Plio-Pleistocene transgressions in the South Caspian Basin, Azerbaijan. Glob. Planet. Chang. 103 (1), 119–134.
Van De Wal, R.S.W., et al., 2011. Reconstruction of a continuous high-resolution CO 2 record over the past 20 million years. Clim. Past 7 (4), 1459–1469.
Vasiliev, I., et al., 2010. The age of the Sarmatian–Pannonian transition in the Transylvanian Basin (Central Paratethys). Palaeogeogr. Palaeoclimatol. Palaeoecol. 297 (1), 54–69.
Vasiliev, I., et al., 2007. Early diagenetic greigite as a recorder of the palaeomagnetic signal in Miocene-Pliocene sedimentary rocks of the Carpathian foredeep (Romania). Geophys. J. Int. 171 (2), 613–629.
Vasiliev, I., et al., 2011. Magnetostratigraphy and radio-isotope dating of upper Miocene-lower Pliocene sedimentary successions of the Black Sea Basin (Taman Peninsula, Russia). Palaeogeogr. Palaeoclimatol. Palaeoecol. 310 (3–4), 163–175.
Vasiliev, I., et al., 2004. Towards an astrochronological framework for the eastern Paratethys Mio-Pliocene sedimentary sequences of the Focşani basin (Romania). Earth Planet. Sci. Lett. 227 (3–4), 231–247.
Vasiliev, I., et al., 2005. Mio-Pliocene magnetostratigraphy in the southern Carpathian foredeep and Mediterranean–Paratethys correlations. Terra Nova 17 (4), 376–384.
Vernigorova, Y.U.V., 2009. Karaganskogo I konkskiy regioyarusy vostochnogo paratetisa: voprosy Ikh ob'yem I stratigraficheskoye samostoyatel'nosti. Geol. Z. 2.
Westerhold, T., et al., 2005. Middle to late Miocene oxygen isotope stratigraphy of ODP Site 1085 (SE Atlantic): New constrains on Miocene climate variability and sea-level fluctuations:. Palaeogeogr. Palaeoclimatol. Palaeoecol. 217, 205–222.
Zijderveld, J.D.A., 1967. AC demagnetization of rocks: analysis of results. Methods Paleomagnetism, pp. 254–286.